Oxygen disorder phenomena in the modulated $Bi_2Sr_2CoO_6$-type structure

1999 J. Phys.: Condens. Matter 11 3997

(http://iopscience.iop.org/0953-8984/11/20/306)

J. Phys.: Condens. Matter **11** (1999) 3997–4008. Printed in the UK PII: S0953-8984(99)98274-7

Oxygen disorder phenomena in the modulated $Bi_2Sr_2CoO_6$-type structure

N Jakubowicz†, D Grebille†§, H Leligny† and M Evain‡

† Laboratoire CRISMAT (UMR CNRS 6508), ISMRA, 14050 Caen Cédex, France
‡ Laboratoire de Chimie des Solides, IMN (UMR CNRS 6502), 44322 Nantes Cédex, France

Received 8 October 1998, in final form 12 February 1999

Abstract. The incommensurate modulated structure of $Bi_{1.91}Sr_2CoO_{5.93}$ ($a = 5.4614(6)$ Å, $b = 5.4471(5)$ Å, $c = 23.415(2)$ Å) with $\vec{q}^* = 0.240(2)\vec{b}^* + \vec{c}^*$ has been refined in the superspace group $F2mm(0\beta1)00s$ using the four-dimensional formalism for modulated structures and single-crystal x-ray diffraction data. Two different regions with different sites for Bi and O atoms are evident along the modulation direction (called M and I regions). The oxygen disorder observed in the M region leads to different possible configurations for [BiO] layers. In particular, a double-chain configuration comparable to the one observed in related compounds is outlined. Therefore, a comparison with related compounds (BiCu or BiFe) is performed.

1. Introduction

Bi-based superconductors of general formula $Bi_2Sr_2Ca_{n-1}Cu_nO_y$ have been widely investigated in recent years, both as regards structural and physical properties [1–6]. All of these phases are characterized by incommensurate structural modulations and several models have been proposed with the aim of providing a better understanding of the relations between these structural modulations and physical properties. One of the main difficulties as regards these structures lies in the description of the charge-reservoir [BiO] layers and in the localization of the different possible oxygen sites. In particular, different atomic sites have been proposed for supplementary oxygen atoms, responsible for the non-stoichiometry of the phase, for the eventual establishing of the modulation via an extension of the Bi–O lattice and for the hole doping of the superconducting CuO_2 layers.

Cationic substitutions of Co or Fe for Cu in the BiSrCaCu oxides have been more recently studied [7–9]. These substitutions lead to a large number of compounds with different structural features.

All of these phases can be described as an intergrowth of rock-salt and perovskite-type layers normal to the *c*-direction. The rock-salt layers always consist of BiO and SrO layers and are common to all of these compounds. Their comparative structural study can be helpful for the understanding of their specific role in the physical properties and in the establishment of the modulated structure. In the Bi–Cu oxides, both $Bi_2Sr_2CuO_6$-type [3] and $Bi_2Sr_2CaCu_2O_8$-type [4] structures are clearly observed and are commonly labelled 2201 and 2212 respectively. It can be noticed that for the Bi–Fe system, evidence has been found only for the 2212 phase [7], and for the Bi–Co system, only for the 2201 one. In this latter case, we could only obtain

§ Author to whom any correspondence should be addressed.

0953-8984/99/203997+12$19.50

poorly crystallized samples of the 2212 phase. The stabilities of these different phases are probably related to the different possible coordinations of Cu, Co and Fe.

For the 2201 phase, we can notice different symmetries according to the substitution, from monoclinic for the Cu compounds to orthorhombic for the Co compounds. This difference of symmetry is related to the stacking of the structural slabs, so it should be interesting to compare the 2201 stacking of the Co system with the orthorhombic 2212 stacking of the Cu system.

The BiSrCo system also exhibits phases with commensurate or incommensurate structural modulations with varying periods on partially replacing Bi by Pb.

The 2201 phase has already been studied [9] and a fourfold supercell model has been given. In the present paper, we propose a new structural study of the same phase using the four-dimensional formalism for modulated phases. Indeed, the magnitude of the modulation vector measured along $\vec{b}^*$ has been found to be significantly different from the simple rational values 0.25 or 0.2, and so was considered as incommensurate. In consequence, as in the case of the Fe compound, the supercell approach can only be approximate. Moreover, recent study of the Fe phases has proved its better efficiency as regards the oxygen atomic sites, probably because of the reduced number of refinement parameters and an optimization of the description of the structural features of the modulation through using periodic modulated functions. Evidence for disorder phenomena has been found in all of the previous studies. It is also interesting to try to clarify the general features of all of these disordered configurations.

2. Experimental procedure

Single crystals of $Bi_2Sr_2CoO_6$ were prepared by the self-flux method using KCl as the flux. A solute was prepared from $Bi(NO_3)_3{\cdot}5H_2O$, $Sr(NO_3)_2$ and $Co(NO_3)_2{\cdot}6H_2O$. These reagents were dispersed in pure water, then evaporated by heating.

The resulting powder was crushed in an agate mortar and then heated at 500 °C in air for 20 h. 75 wt% KCl was added and the whole was heated at 1100 °C for 2 h, rapidly cooled to 950 °C and then slowly cooled to 750 °C at 2 °C h^{-1}. A monodomain single crystal was mechanically isolated from the solidified material after dissolving the KCl in warm water.

In a first stage, the crystal quality of the sample was tested with a Weissenberg camera. A first estimate of the crystal parameters and symmetry was obtained. Diffuse scattering streaks along $\vec{c}^*$, between satellite reflections, were also observed. These results still indicate a stacking disorder of the material.

A platelet crystal ($0.300 \times 0.200 \times 0.010$ mm^3) was then mounted on an Enraf-Nonius CAD-4 diffractometer. The cell parameters, $a = 5.4614(6)$ Å, $b = 5.4471(5)$ Å, $c = 23.415(2)$ Å, were refined by accurate centring of 25 reflections. The intensities of the main and satellite reflections up to the second order were measured at room temperature. No significant variation of the intensity of three standard reflections was detected. 1170 independent reflections with $I > 3\sigma(I)$ were measured using Mo Kα radiation. They were first corrected for Lorentz and polarization effects and then an absorption correction based on the crystal morphology was applied. Both a profile analysis and a least-squares refinement of the θ-angles confirmed the value of 0.240(2) for the q_2^*-component of the modulation wavevector, significantly different from the simple rational value 0.25.

This data collection was then completed by the use of a STOE image plate detector in order to improve the $I/\sigma(I)$ ratio, and so the quality of the data set. 245 independent reflections with $I > 3\sigma(I)$ were measured by this method (because of the restriction in $\sin(\theta)/\lambda$ due to the system configuration). The two sets of reflections (CAD-4 and image plate) were rescaled using 242 common reflections with $I > 3\sigma(I)$ and gathered.

The final data set consists of 1188 reflections with satellite reflections up to second order. We can notice that the introduction of the set of reflections measured by the image plate (with a better $I/\sigma(I)$ ratio) leads to a significant improvement of the agreement factor, probably because of a high redundancy and longer exposure times.

The experimental data are summarized in table 1.

Table 1. Experimental data.

Crystal formula	$Bi_{1.91}Sr_2CoO_{5.88}$
Crystal size (mm^3)	$0.300 \times 0.207 \times 0.010$
Cell parameters (Å)	$a = 5.4614(6)$, $b = 5.4471(5)$, $c = 23.415(2)$
T (K)	294
Modulation wavevector	[0, 0.240(2), 1]
Superspace group	$F2mm(0\beta1)00s$
Z	4
Data collection	Enraf-Nonius CAD-4 diffractometer/STOE IPDS
Wavelength (Å)	λ(Mo Kα) = 0.71073
Registered space	CAD4: $0 < h < 10, -10 < k < 10, 0 < l < 46, -2 < m < 2$ IPDS: $0 < h < 4, -4 < k < 5, 0 < l < 22, -2 < m < 2$
No of measured reflections	CAD4: 3903 IPDS: 373
No of reflections with $I > 3\sigma(I)$	CAD4: $h\,k\,l\,0$: 244; $h\,k\,l\,\pm1$: 529; $h\,k\,l\,\pm2$: 398 IPDS: $h\,k\,l\,0$: 72; $h\,k\,l\,\pm1$: 73; $h\,k\,l\,\pm2$: 98
No of refinement parameters	114
R, wR ($h\,k\,l\,m$)	0.042, 0.044
R, wR ($h\,k\,l\,0$)	0.043, 0.044
R, wR ($h\,k\,l\,1$)	0.039, 0.042
R, wR ($h\,k\,l\,2$)	0.045, 0.050

3. Structural refinement

The modulated structure was refined within the four-dimensional formalism for modulated structures using the JANA program [10]. The atomic positions in the nth cell can be expressed as follows:

$$\vec{r}_n = \vec{r}_n^{\,0} + \sum_{m,i} (A_{i,m} \sin(2m\pi\overline{x}_4) + B_{i,m} \cos(2m\pi\overline{x}_4))\vec{a}_i \tag{1}$$

where $\vec{r}_n^{\,0}$, is the average atomic position in the nth cell, $A_{i,m}$ and $B_{i,m}$ are the Fourier terms of the displacement modulation functions and $\overline{x}_4 = \vec{q} \cdot \vec{r}_n^{\,0} + t$ is the internal parameter. In the same way, the thermal modulations can be written as [11]

$$U_{ij}(\overline{x}_4) = \sum_m (u_{ij,m} \sin(2m\pi\overline{x}_4) + v_{ij,m} \cos(2m\pi\overline{x}_4)). \tag{2}$$

The observed reflection conditions ($H\,K\,L\,m$, $H + K = 2n$, $H + L + m = 2n$ and $K + L + m = 2n$) lead to the Bravais class $mmmF(0\beta1)$. The supplementary condition $m = 2n$ observed for the $H\,K\,0\,m$ reflections reveals the existence of a glide mirror $\binom{m_z}{s}$. As a consequence, the phases of the modulation function of the related sites are opposite. The refinement was first carried out assuming the centrosymmetric superspace group $Fmmm(0\beta1)00s$.

A starting model was deduced from the structural results available for analogous structures. It can be described as a stacking along $\vec{z}$ of BiO and SrO rock-salt-type layers with the

intercalation of a CoO_2 perovskite-type layer. In the following, the respective oxygen atoms of the [BiO], [SrO] and [CoO_2] layers will be labelled OB, OS and OC.

As in the previous structure refinements of related compounds, it was not possible to describe the Bi and O atoms of the BiO layers, throughout the phase range, with only one atomic Bi or O site. In fact, a second bismuth site, Bi_2, was evident on the x_3–x_4 Fourier map at $x_1 = 0.015$ and $x_2 = 0$, replacing the first Bi_1 site in the range $x_4 = 0.2$–0.3. To take into account the alternate occupation of these two different sites, a harmonic occupation modulation function was introduced for them, expressed as

$$P(\overline{x}_4) = P_0 + \sum_m (A'_m \sin(2m\pi\overline{x}_4) + B'_m \cos(2m\pi\overline{x}_4)). \tag{3}$$

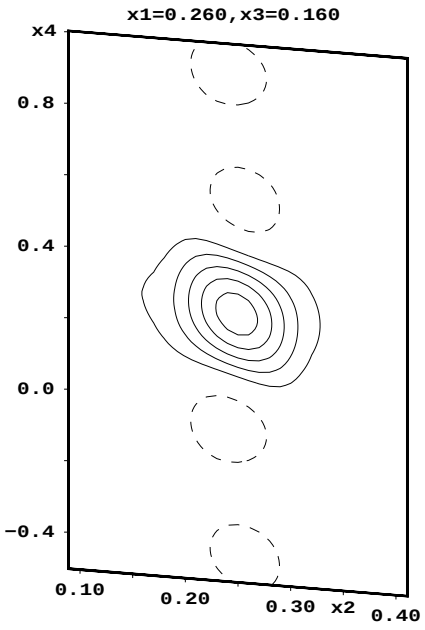

Figure 1. An x_2–x_4 section of the difference Fourier map. Contours are drawn at intervals of 1 electron Å^{-3}.

In the same way, the observation of difference Fourier maps for the same phase range still revealed an electronic density at $x_1 = 0.26$ and $x_3 = 0.16$ (see figure 1), which had not been taken into account. We then introduced in this range a specific oxygen atom OB_2. This light oxygen electronic density, defined in a reduced interval, could only be refined, for convergence criteria, by a crenel function. Indeed, only two parameters (Δ and x_4^0) are to be refined. The occupancy is set to 1 over an interval of length Δ centred on x_4^0. Δ and x_4^0 were refined to 0.07 and 0.25 respectively. This crenel function model appeared not to be convenient for the Bi_2 atom, probably because of the significant weight of the corresponding electronic density, of its larger existence domain and of a likely disorder phenomenon here described as a partial occupation of the Bi_1 and Bi_2 sites. The introduction of these Bi_2 and OB_2 sites allowed a significant improvement of the global R-factor to be achieved. Nevertheless, the introduction of the OB_2 atom leads to unrealistic OB_2–OS distances (<2.6 Å). So, we also refined the occupation of the OS atom with a crenel function. We find vacant OS sites around $x_4 = 0.25$ which correspond to the appearance of OB_2.

The x_1–x_2 section of the difference Fourier map clearly shows a splitting of the main oxygen site (OB_1) of the BiO layer into two disordered sites OB_{1a} and OB_{1b}, separated by more than 1 Å, symmetry related in the basic $Fmmm$ group. These two sites exist throughout,

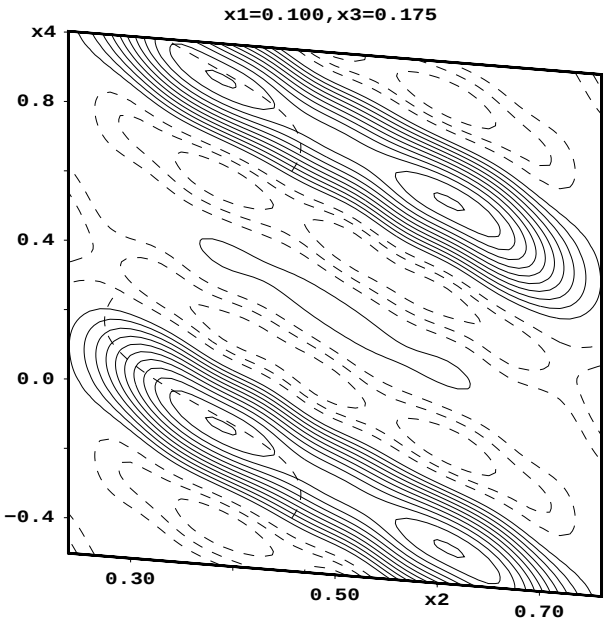

Figure 2. An x_2–x_4 section of the difference Fourier map. Contours are drawn at intervals of 1 electron $Å^{-3}$.

except in the range $x_4 = 0.20$–0.30 (figure 2). This range corresponds to the full occupancy of the OB_2 site. Their constrained occupation is close to 0.5. The refinement in the polar superspace group $F2mm(0\beta1)00s$ did not permit us to avoid this splitting, but improved the R-factor. Moreover, the Hamilton test [14] leads to the conclusion that the symmetry lowering from $Fmmm$ to $F2mm$ is significant (at the 0.005 level). The refinement was then carried out in the polar group.

Furthermore, in our study, the x_2–x_4 section of the difference Fourier map at $x_1 = 0.1$ and $x_3 = 0.17$ (see figure 2) shows a large amplitude of modulation for OB_1 atoms along $\vec{b}$. We decided to model this density with two symmetry-related oxygen atoms alternately occupying sites on either side of the m_y-mirror, which conforms with the interpretation previously proposed for the BiFe-2212 compound [7]. Such a description of the electronic density allows us to have displacive terms that are comparable for OB_1 and Bi atoms.

In the final refinement, Bi_1, Bi_2, Sr and OS are located at (8d) sites, Co at (4a) sites, OC at (8c) sites, OB_{1a}, OB_{1b} and OB_2 at (16e) sites. Anisotropic atomic displacement temperature factors were taken for cations and isotropic ones for oxygen. Finally, a modulation of these terms was also introduced for cations, leading to a significant improvement of the R-factors, defined by

$$R = \left(\sum |F_o - F_c|\right) \Big/ \left(\sum F_o\right)$$
$$wR = \left[\left(\sum_w (|F_o| - |F_c|)^2\right) \Big/ \left(\sum_w |F_o|^2\right)\right]^{1/2}. \tag{4}$$

The final global agreement factor in $F2mm(0\beta1)00s$ is $R = 0.042$ with $R_0 = 0.043$ for the main reflections, and $R_1 = 0.039$ and $R_2 = 0.045$ for the first- and second-order satellites respectively, for 114 refinement parameters (the equivalent agreement factors in the case of the centrosymmetric group were $R_0 = 0.048$, $R_1 = 0.042$, $R_2 = 0.052$ respectively for 86 refinement parameters). The refinement results are given in table 2, table 3 and table 4.

Table 2. Positional (A_i) and occupational (A'_i) Fourier parameters (see equations (1) and (3)). The zeros $0^\star$ were fixed during the refinement because they are not significant. The zeros $0^\dagger$ were constrained by symmetry.

		$A_0(P_0)$	$A_1(A'_1)$	$B_1(B'_1)$	$A_2(A'_2)$	$B_2(B'_2)$
Bi_1	U_1	$0^\star$	−0.008(1)	$0^\dagger$	$0^\dagger$	0.0085(9)
	U_2	$0^\dagger$	$0^\dagger$	−0.09959(9)	−0.0158(2)	$0^\dagger$
	U_3	0.18703(5)	0.0127(1)	$0^\dagger$	$0^\dagger$	0.00021(9)
	P	0.794(2)	−0.346(2)	$0^\dagger$	$0^\dagger$	0.300(2)
Bi_2	U_1	0.015(1)	0.016(2)	$0^\dagger$	$0^\dagger$	0.029(2)
	U_2	$0^\dagger$	$0^\dagger$	−0.093(2)	0.045(1)	$0^\dagger$
	U_3	0.1940(4)	−0.0013(4)	$0^\dagger$	$0^\dagger$	−0.0072(4)
	P	0.159(2)	0.315(2)	$0^\dagger$	$0^\dagger$	−0.251(3)
Sr	U_1	0.5016(8)	$0^\star$	$0^\dagger$	$0^\dagger$	$0^\star$
	U_2	$0^\dagger$	$0^\dagger$	−0.0566(3)	−0.0143(3)	$0^\dagger$
	U_3	0.07623(5)	0.0248(1)	$0^\dagger$	$0^\dagger$	−0.00229(8)
Co	U_1	$0^\star$	$0^\dagger$	$0^\dagger$	$0^\dagger$	0.006(2)
	U_2	$0^\dagger$	$0^\dagger$	$0^\dagger$	−0.0044(7)	$0^\dagger$
	U_3	$0^\dagger$	0.0319(2)	$0^\dagger$	$0^\dagger$	$0^\dagger$
OC	U_1	0.261(4)	$0^\dagger$	$0^\dagger$	−0.005(2)	$0^\star$
	U_2	0.2500	$0^\dagger$	$0^\dagger$	$0^\star$	$0^\star$
	U_3	$0^\dagger$	0.0202(3)	$0^\star$	$0^\dagger$	$0^\dagger$
OS	U_1	0.009(3)	0.03(1)	$0^\dagger$	$0^\dagger$	0.02(1)
	U_2	$0^\dagger$	$0^\dagger$	−0.082(2)	−0.033(2)	$0^\dagger$
	U_3	0.0995(4)	0.0127(8)	$0^\dagger$	$0^\dagger$	−0.0017(8)
	Δ, x_4	0.85(1)	0.75			
OB_{1a}	U_1	0.109(3)	0.017(5)	0.014(6)		
	U_2	0.371(4)	−0.089(5)	−0.029(6)		
	U_3	0.1783(8)	0.016(1)	$0^\star$		
	P	0.22(1)	−0.11(2)	0.40(2)		
OB_{1b}	U_1	−0.080(3)	0.025(5)	0.008(5)		
	U_2	0.383(5)	−0.094(7)	−0.074(8)		
	U_3	0.1924(8)	0.021(1)	$0^\star$		
	P	0.26(2)	−0.01(2)	0.22(3)		
OB_2	U_1	0.276(7)				
	U_2	0.2500				
	U_3	0.1667(8)				
	Δ, x_4	0.077(5)	0.25			

4. Results

The general structural features of this 2201 phase have been described previously [9] and are confirmed here, as will be illustrated further. Nevertheless, a more accurate determination of the oxygen-atom location now allows a better description of the various cation environments to be given. In particular, it is not possible to account for the atomic positions in the BiO layers with a continuous model, and alternation of specific regions is evident along the modulation direction (figure 3).

In fact, the study of the Bi–O layers led us to introduce two types of atomic site for Bi and

Table 3. Thermal parameters (Å^2). Non-diagonal terms are fixed to 0.

	U_{iso}	U_{11}	U_{22}	U_{33}
Bi_1	0.0126(2)	0.0194(4)	0.0093(5)	0.0092(3)
Bi_2	0.0096(4)	0.0147(9)	0.0018(5)	0.0122(7)
Sr	0.0138(3)	0.0135(4)	0.0116(5)	0.0164(8)
Co	0.0116(9)	0.0056(8)	0.0082(6)	0.021(2)
OC	0.021(1)			
OS	0.014(1)			
OB_{1a}	0.003(2)			
OB_{1b}	0.008(3)			
OB_2	0.003(3)			

Table 4. Thermal parameters (Å^2) (see equation (2)). The zeros $0^\star$ were fixed during the refinement because they are not significant. The zeros $0^\dagger$ were constrained by symmetry.

		$u_{ij,1}$	$v_{ij,1}$	$u_{ij,2}$	$v_{ij,2}$
Bi_1	U_{11}	−0.0162(3)	$0^\dagger$	$0^\dagger$	0.0162(4)
	U_{22}	0.0157(3)	$0^\dagger$	$0^\dagger$	−0.0046(1)
	U_{33}	−0.0042(3)	$0^\dagger$	$0^\dagger$	0.0028(3)
	U_{12}	$0^\dagger$	$0^\star$	−0.0060(9)	$0^\dagger$
	U_{13}	−0.0050(6)	$0^\dagger$	$0^\dagger$	−0.002(1)
	U_{23}	$0^\dagger$	0.0019(2)	−0.0031(2)	$0^\dagger$
Sr	U_{11}	0.0335(5)	$0^\dagger$	$0^\dagger$	−0.0039(7)
	U_{22}	0.0143(4)	$0^\dagger$	$0^\dagger$	−0.0101(5)
	U_{33}	$0^\star$	$0^\dagger$	$0^\dagger$	−0.0169(7)
	U_{12}	$0^\dagger$	0.007(1)	0.009(1)	$0^\dagger$
	U_{13}	0.012(1)	$0^\dagger$	$0^\dagger$	−0.005(1)
	U_{23}	$0^\dagger$	0.0110(5)	−0.0021(4)	$0^\dagger$
Co	U_{11}	$0^\dagger$	$0^\dagger$	$0^\dagger$	$0^\star$
	U_{22}	$0^\dagger$	$0^\dagger$	$0^\dagger$	−0.0085(9)
	U_{33}	$0^\dagger$	$0^\dagger$	$0^\dagger$	−0.009(1)
	U_{12}	$0^\dagger$	$0^\dagger$	−0.004(2)	$0^\dagger$
	U_{13}	0.008(2)	$0^\dagger$	$0^\dagger$	$0^\dagger$
	U_{23}	$0^\dagger$	0.004(1)	$0^\dagger$	$0^\dagger$

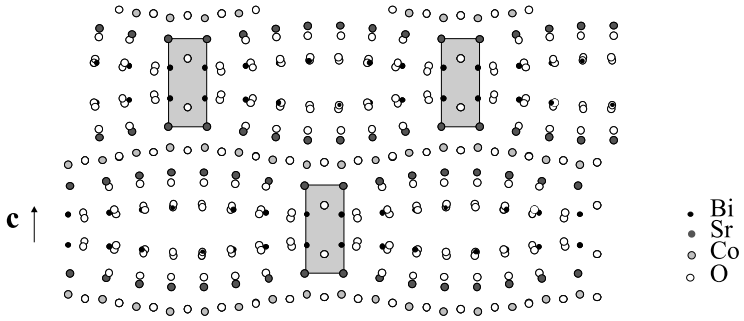

Figure 3. The projection along $\vec{a}$ of the structure. Shadowed regions correspond to the I zones (see the text).

O: Bi_1 and OB_1 are characterized by continuous displacive modulation functions which are defined, according to the occupation modulation functions, in approximatively four contiguous cells out of five, defining modulated regions (called M regions). In these regions, the modulated displacements are very close to linear ones and look like similar displacements in the BiCu-2212 or BiFe-2212 compounds. Between these M regions, Bi_2 and OB_2 are present in only one cell, defining an intermediate zone (called the I region) with a special configuration, which cannot be accounted for in a general modulation scheme. The I regions here play a similar role of accommodation to the disordered regions previously described in the Bi–Fe or Bi–Cu 2212 structures [4, 7]. The main difference is now that these latter zones are no longer characterized by any obvious disorder, while in the M regions a new and important disorder along the x-direction is now present in the oxygen configuration.

4.1. Description of the M zones

As far as cations are concerned, we observe in these regions an almost perfect equivalence between the atomic positions refined in the previous supercell description [9] and the present ones deduced from a modulated scheme (figure 4(a), figure 4(b)). The main difference is that the supercell description particularizes a finite number of independent sites while the incommensurate character of the structure theoretically allows an infinity of sites characterized by the continuous modulation function. Nevertheless, we have to keep in mind that the deviation from a commensurate structure is small and so the supercell description is a good approximant to the real structure. The displacement amplitudes increase from Bi to Co along $\vec{c}$ while they increase from Co to Bi along $\vec{b}$, as was already observed for the BiCu-2212, BiFe-2212 and BiCu-2201 phases. Nevertheless, the displacement amplitude along $\vec{c}$ is much greater than in the related phases (0.2 Å for Bi and 0.35 Å for Cu in BiCu-2212, while it reaches 0.3 Å for Bi and 0.7 Å for Co in our phase). This difference in the amplitudes of displacement along $\vec{c}$, coupled with a shorter modulation period along $\vec{b}$ (22.5 Å against 25.7 Å) results in a more contrasted picture of the two 'lips' of the double BiO layers in the projection along $\vec{a}$ (figure 3). The interlayer distances are now longer in the M zones and shorter in the I zones, and this different configuration in the $(\vec{b}, \vec{c})$ plane probably correlates with the different configuration of the BiO layer in the (a, b) plane, which will be described now.

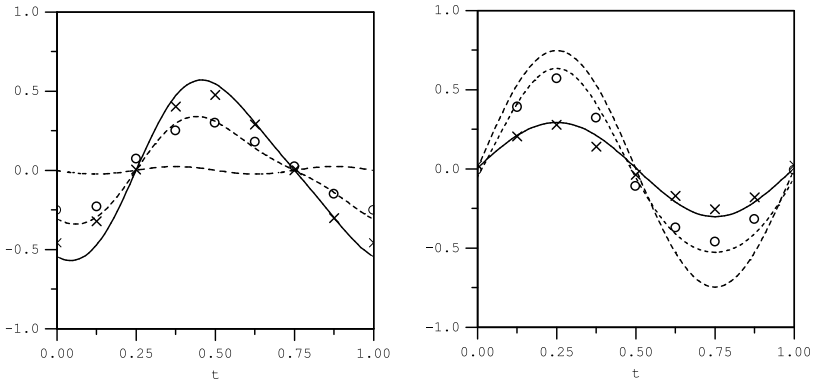

Figure 4. Relative displacive modulation functions along $\vec{y}$ (a) and along $\vec{z}$ (b) versus the phase variable t for cations. Curves represent the results from this study: solid curve: Bi; dashed curve: Sr; dotted curve: Co. Crosses represent Bi and circles Sr in the supercell study.

For the oxygen atoms, the comparison with the previous study is not so clear because of a large degree of uncertainty and a large dispersion of the results in the supercell study. The oxygen disorder mentioned in the previous supercell study (rock-salt arrangement) is confirmed but the modulated approach now allows a better description of these atoms to be given: this is clearly outlined by the cation–oxygen distances. Some distances calculated in the supercell model are too short (for example a Co–O distance of 1.69 Å) while they always have reasonable values (from 1.89 to 2.38 Å for Bi–O, from 2.56 to 2.93 Å for Sr–O and from 1.88 to 2.33 Å for Co–O distances) in the modulated model.

The important disorder introduced for OB_1 atoms leads to a configuration of [BiO] layers rather different to that in the BiFe-2212 or BiCu-2212 compounds. In these phases, the ordered zone, which corresponds to the M region in this study, shows a characteristic configuration in double chains along the modulation direction with pairs of parallel curves for Bi–Bi interatomic distances. In our phase, Bi–Bi interatomic distances, which are represented by identical curves, involve a particular configuration with Bi atoms almost equidistant in the *a–b* plane (3.6–3.8 Å apart). So, [BiO] layers cannot be described any longer in terms of double chains. Contrary to the case for the 2212 compounds, oxygen atoms seem to accommodate the more symmetrical Bi configuration thanks to the two different sites OB_{1a} and OB_{1b}.

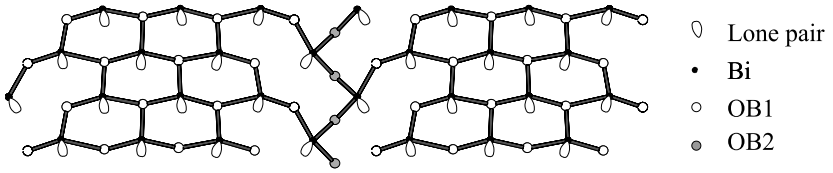

Figure 5. The honeycomb configuration of the BiO layer. Only OB_{1a} sites are occupied. BiO interatomic distances <2.6 Å are represented by solid lines.

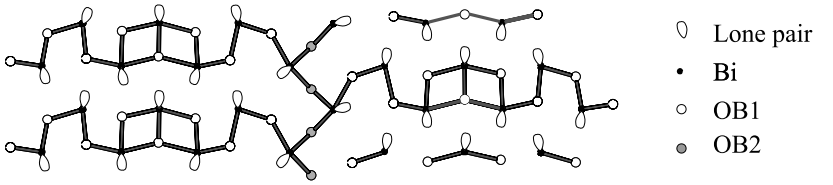

Figure 6. The double-chain configuration of the BiO layer. OB_{1a} and OB_{1b} sites are alternately occupied. BiO interatomic distances <2.6 Å are represented by solid lines.

When considering one BiO layer and all possible sites for oxygen; it is obvious that not all local configurations are possible, and that the two OB_{1a} and OB_{1b} sites cannot be simultaneously occupied. It is then possible to imagine different configurations. For example, the simultaneous occupation of all OB_{1a} sites would correspond to a 'honeycomb' ordering of Bi and OB atoms along the modulation direction (figure 5). The alternate occupation of OB_{1a} and OB_{1b} sites in every subcell along the modulation direction gives another configuration which looks very similar to the double-chain configuration of the BiFe-2212 or BiCu-2212 compounds (figure 6) with Bi–O distances less than 2.5 Å inside a double chain. When considering the Bi environment and the location of the electronic lone pair Lp [12] more accurately using electrostatic equilibrium models, we find in all cases one almost constant Bi–OS distance (around 2.08 Å), Bi–OB_1 distances varying from 2.10 to 2.60 Å and a Bi–Lp distance in the range 0.6–0.9 Å (see table 5, table 6 and table 7 for the double-chain

configuration). All of the distances are compatible with the known Bi configurations, but the 'honeycomb' arrangement leads to an angular configuration with O–Bi–O angles greater than 90° for these short bond lengths and such configurations were not observed in the related compounds.

Table 5. The main interatomic Bi–O distances (Å) and $\widehat{\text{O–Bi–O}}$ angles (degrees) in the M region in the double-chain-configuration hypothesis.

Bi_{1a-2}	OS_{a-2}	OB_{1an-2}	OB_{1m-2}	OB_{1m-3}	Lp_1
OS_{a-2}	**2.09**	3.06	2.98	3.16	2.70
OB_{1an-2}	90	**2.23**	2.90	2.92	2.75
OB_{1m-2}	85	79	**2.31**	4.76	2.58
OB_{1m-3}	84	74	151	**2.61**	2.91
Lp_1	134	135	102	105	**0.78**

Table 6. The main interatomic Bi–O distances (Å) and $\widehat{\text{O–Bi–O}}$ angles (degrees) in the M region in the double-chain-configuration hypothesis.

Bi_{1a-3}	OS_{a-3}	OB_{1ab-2}	OB_{1a-3}	OB_{1m-3}	Lp_3
OS_{a-3}	**2.02**	3.05	3.00	3.06	2.67
OB_{1ab-2}	94	**2.16**	2.81	2.84	2.80
OB_{1a-3}	85	76	**2.41**	4.66	2.73
OB_{1m-3}	87	77	150	**2.41**	2.72
Lp_3	133	133	104	103	**0.84**

Table 7. The main interatomic Bi–O distances (Å) and $\widehat{\text{O–Bi–O}}$ angles (degrees) in the M region in the double-chain-configuration hypothesis.

Bi_{1a-4}	OS_{a-4}	OB_{1a-4}	OB_{1ab-3}	Lp_3
OS_{a-4}	**2.09**	2.97	3.15	2.60
OB_{1a-4}	88	**2.19**	3.10	2.45
OB_{1ab-3}	88	85	**2.42**	2.67
Lp_3	135	106	134	**0.66**

The apparent disorder in the oxygen configuration of the BiO layers could be explained by a random stacking of M zones either in the *c*-direction from one slab to the other or in the *b*-direction from one side of the I zone to the other.

In this M zone, Co has a standard octahedral coordination (equatorial distances: 1.89, 1.91, 19.4 and 1.96 Å and two apical Co–O distances that are slightly asymmetric: 2.2 and 2.5 Å) and Sr is surrounded by nine oxygen atoms.

4.2. Description of the I zones

In this intermediate region, corresponding to the disordered zone of the 2212 compounds, we introduced a second bismuth site (Bi_2), shifted along $\vec{x}$ from the Bi_1 site, according to the x_4-value. Furthermore, OB_1 atoms are replaced by OB_2 atoms.

This zone corresponds to the bridging one of the supercell study [9]. In this model, a ninth oxygen atom was introduced for every eight bismuth. This supplementary oxygen is accounted for here by the new site symmetry and occupation of the OB_2 site.

Table 8. The main interatomic Bi–O distances (Å) and $\widehat{\text{O–Bi–O}}$ angles (degrees) in the I region.

Bi_{2a-4}	OB_{2b-4}	OB_{2m-1}	OB_{1n-1}	Lp_{13}
OB_{2b-4}	**2.01**	2.73	2.76	2.56
OB_{2m-1}	82	**2.13**	3.26	2.23
OB_{1n-1}	77	153	**2.40**	2.66
Lp_{13}	166	92	112	**0.56**

We find vacant OS sites around $x_4 = 0.25$ which corresponds to the zone of appearance of OB_2. This result has already been observed for the copper compound [3]. As a result, all O–O distances reach reasonable values greater than 2.67 Å and the Bi_2 environment is much more symmetric that those encountered in M zones (table 8). This latter environment looks like the Bi(a) environment in the transition region of the collapsed BiFe oxide phase [8].

Note that the occurrence of OB_2 corresponds to the zone where Bi_2 replaces a Bi_1 atom. Moreover, in contrast to the case for the related Fe or Cu phases, one cannot observe any disorder for Bi and O atoms in this I region. This region could allow, via the intermediate of OB_2 and Bi_2, an important disorder from one M region to another. Such a disorder is postulated in figure 6.

Considering now CoO and SrO layers, we notice that the absence of OS in the [SrO] layer modifies the cationic environments. For example, it implies a square-pyramidal environment for Co instead of the usual octahedral one. The bond valence of Co has also been calculated [13]; we obtain 2.5 for the octahedral environment of the M zones and 2.0 for the pyramidal one of the I zone. We notice that, in the square-pyramidal environment, the apical Co–O distance is quite long (2.77 Å), which leads to a nearly planar environment. Sr is sevenfold coordinated in this zone ($v = 1.78$) because of the absence of OS and eightfold coordinated ($v = 1.92$) at the boundary of the M and I zones. The previous calculated cationic valences and their respective occurrences in the modulated crystal, weighted by the refined occupancy of the respective atomic sites, correspond to the formula $Bi_{1.91}Sr_2CoO_x$. This should lead to an x-value for oxygen of 5.85. The weight of oxygen in the present refinement of the x-ray diffraction data is rather weak and can only provide an estimate of x. So, taking into account the respective occupations of the OC, OB_{1a} and OB_{1b} sites and the relative range of existence of the OS and OB_2 sites, the result for x from the refinement parameters is 5.93(7), close to the previous value. The same result is obtained when considering the nominal valences +3, +2, +2 for Bi, Sr and Co respectively.

5. Conclusions

The previously mentioned disorder in the oxygen configuration of the BiO layers of the BiCo-2201 compound has been investigated again here. The alternation of different regions (rock-salt or M regions and bridging or I regions) is confirmed. The usual appearance of double BiO layers is still observed, but with a more pronounced contrast due to larger modulation amplitudes in the stacking direction. This different stacking is probably related to the different configurations in the Bi and O arrangement in a layer. Even if no trace of the usual BiO double chains, characterizing the BiCu or BiFe compounds, has been found at the Bi location, the oxygen disordered position allows us to postulate the existence of possible double-chain configurations compatible with the known Bi environments implied for all related compounds. The apparent disorder evident from the structural study is probably the result of a random stacking of such configurations either in the stacking or in the modulation direction.

Acknowledgments

The authors wish to acknowledge Professor D Groult for providing crystals and are greatly indebted to Professor B Raveau for helpful discussions.

References

[1] Michel C, Hervieu M, Borel M M, Grandin A, Deslandes F, Provost J and Raveau B 1988 *Z. Phys.* B **68** 421
[2] Hervieu M, Michel C, Domenges B, Lalignant Y, Lebail A, Ferey G and Raveau B 1988 *Prog. High Temp. Supercond.* **7** 159
[3] Leligny H, Durĉok S, Labbé Ph, Ledesert M and Raveau B 1992 *Acta Crystallogr.* B **48** 407
[4] Grebille D, Leligny H, Ruyter A, Labbé Ph and Raveau B 1996 *Acta Crystallogr.* B **52** 628
[5] Petříček V, Gao Y, Lee P and Coppens P 1990 *Phys. Rev.* B **42** 4228
[6] Yamamoto A, Onoda M, Takayama-Muromachi E and Izumi F 1990 *Phys. Rev.* B **42** 4228
[7] Pérez O, Leligny H, Grebille D, Grenêche J M, Labbé Ph, Groult D and Raveau B 1997 *Phys. Rev.* B **55** 1236
[8] Pérez O, Leligny H, Grebille D, Baldinozzi G, Graafsma H, Labbé Ph and Groult D 1997 *Phys. Rev.* B **56** 5662
[9] Tarascon J M, Miceli P F, Barboux P, Hwang D M, Hull G W, Giroud M, Greene L H, LePage Y, McKinnon W R, Tselepis E, Pleizier G, Eibschutz M, Neumann D A and Rhyne J J 1989 *Phys. Rev.* B **39** 11 587
[10] Petříček V 1998 *Crystallographic Computing System JANA98* Institute of Physics, Academy of Sciences of the Czech Republic, Prague
[11] Jansen T, Janner A, Looijjenga-Vos A and De Wolff P 1992 *International Tables for Crystallography* (Dordrecht: Kluwer)
[12] Jakubowicz N, Pérez O, Grebille D and Leligny H 1998 *J. Solid State Chem.* **139** 194
[13] Brese N E and O'Keefe M 1991 *Acta Crystallogr.* B **47** 192
[14] Hamilton W C 1965 *Acta Crystallogr.* **18** 502